



Published in final edited form as:

*Adv Exp Med Biol.* 2010 ; 664: 309–316. doi:10.1007/978-1-4419-1399-9\_35.

## Spectral Domain Optical Coherence Tomography and Adaptive Optics: Imaging Photoreceptor Layer Morphology to Interpret Preclinical Phenotypes

Jungtae Rha, Adam M. Dubis, Melissa Wagner-Schuman, Diane M. Tait, Pooja Godara, Brett Schroeder, Kimberly Stepien, and Joseph Carroll

Department of Ophthalmology; Department of Cell Biology; Neurobiology, and Anatomy; Department of Biophysics, Medical College of Wisconsin, The Eye Institute, Milwaukee, WI, USA

### Abstract

Recent years have seen the emergence of advances in imaging technology that enable in vivo evaluation of the living retina. Two of the more promising techniques, spectral domain optical coherence tomography (SD-OCT) and adaptive optics (AO) fundus imaging provide complementary views of the retinal tissue. SD-OCT devices have high axial resolution, allowing assessment of retinal lamination, while the high lateral resolution of AO allows visualization of individual cells. The potential exists to use one modality to interpret results from the other. As a proof of concept, we examined the retina of a 32 year-old male, previously diagnosed with a red-green color vision defect. Previous AO imaging revealed numerous gaps throughout his cone mosaic, indicating that the structure of a subset of cones had been compromised. Whether the affected cells had completely degenerated or were simply morphologically deviant was not clear. Here an AO fundus camera was used to re-examine the retina (~6 years after initial exam) and SD-OCT to examine retinal lamination. The static nature of the cone mosaic disruption combined with the normal lamination on SD-OCT suggests that the affected cones are likely still present.

### 35.1 Introduction

Human trichromacy relies on three different cone types in the retina; long- (L), middle- (M), and short- (S) wavelength-sensitive. Dichromatic color vision results from the functional loss of one cone class. One central question has been whether individuals with this form of red-green color-blindness have lost one population of cones or whether they have normal numbers of cones filled with either of two instead of three pigments. It has become clear that the answer to this question depends upon the genotype. Two main causes of inherited red-green color vision deficiency have been identified. The most common cause is rearrangement of the L/M opsin genes (Xq 28) resulting either in the deletion of all but one visual pigment gene, or in the production of a gene array in which the first two genes both encode a pigment of the same spectral class (Deeb et al. 1992; Jagla et al. 2002; Nathans et al. 1986; Neitz et al. 2004; Ueyama et al. 2003). The second general cause is the introduction of an inactivating mutation in either the first or second gene in the array.

These two different causes of inherited color vision defects might be expected to lead to different retinal phenotypes. It is thought that all photoreceptors destined to become L or M cones will express either the first or second gene in the X-chromosome array (Hayashi et al.

1999). In the case of gene rearrangements, all cone photoreceptors are expected to express a gene that encodes a functional pigment. However in the case of the inactivating mutation, a fraction of the photoreceptors will express a pigment that is not functional and, in fact, may be deleterious to the viability of the cell. Recently it was discovered that there are different retinal phenotypes among red-green color blind individuals. Carroll et al. (2005) found that in individuals having either a single-gene array, or an array in which the first two genes both encode a pigment of the same spectral class, the cone mosaic is normal in appearance. In contrast, in an individual with a deuteranopic phenotype in whom the M-opsin gene (OPN1MW; MIM:303800) in the array encoded a pigment with an inactivating mutation, a dramatic loss of healthy cones was observed. This is consistent with the authors' hypothesis that cells expressing the mutant pigment degenerated (Carroll et al. 2004).

Here we re-examined this individual with a disrupted cone mosaic using adaptive optics (AO) to determine whether there has been any change in the appearance of the cone mosaic over time. In addition, we evaluated the photoreceptor layer using spectral domain optical coherence tomography (SD-OCT) in an effort to deduce whether the cones expressing the mutant pigment degenerated completely or whether they have simply been functionally compromised. AO and SD-OCT provide complementary views of the living retina, and efforts to advance our understanding on how the images from these two modalities relate to one another will improve the clinical utility of each.

## 35.2 Materials and Methods

### 35.2.1 Subjects

A 32 year old male (NC) was previously reported as having a novel M-opsin sequence in transmembrane IV (leucine 153, isoleucine 171, alanine 174, valine 178, alanine 180; 'LIAVA') (Carroll et al. 2004; Neitz et al. 2004). Initial examination took place in January of 2003, with first follow-up in December of 2004, and the most recent exam in November of 2008. Complete ophthalmic exam revealed no abnormalities at any of the three visits. Best-corrected visual acuity was 20/16. Retinal imaging was done using adaptive optics and SD-OCT (see below). Sixty individuals with clinically normal vision were imaged using Bioptigen™ SD-OCT as controls for outer nuclear layer analysis. Written informed consent was obtained from all subjects. The study conforms to the Declaration of Helsinki and was approved by the Children's Hospital of Wisconsin Institutional Review Board.

### 35.2.2 Adaptive Optics Retinal Imaging

Images of NC's cone mosaic were obtained using a newly developed AO ophthalmoscope housed at the Medical College of Wisconsin. The head was stabilized using a dental impression on a bite bar. The subject's eye was dilated and accommodation suspended through use of a combination of Phenylephrine Hydrochloride (2.5%) and Tropicamide (1%). In a continuous closed-loop fashion, the eye's monochromatic aberrations were measured over a 6.8-mm pupil with a Shack-Hartmann wavefront sensor and corrected for them with a 52-channel deformable mirror (Imagine Eyes, Orsay, France). Details on the Mirao52 deformable mirror have been previously published (Fernández et al. 2006).

Once a wavefront correction was obtained, a retinal image was acquired by illuminating the retina with a 1.8° diameter, 500 ms flash. A fiber-coupled near infrared source was used for imaging, which consists of a 200 mW SLD (center wavelength of 837.8 nm, 14.1-nm spectral bandwidth FWHM) and 110 m of multimode step index fiber (Fiberguide Industries, Stirling, NJ USA). The optical role of the fiber was to reduce the spatial coherence of the laser and prevent speckle noise that confounds interpretation of the retinal image. The fiber has a 0.22 numerical aperture, core diameter of 365 μ and core refractive

index of 1.457 at 0.633 nm wavelength. The function of the step index multimode fiber has been described in detail (Rha et al. 2006). The exposure at the cornea was 2 mW, well below the maximum permissible exposure for continuous intrabeam viewing recommended by ANSI (Z136 2007). A back-illuminated scientific-grade 12-bit charge-coupled device (CCD) (Cam1M100-SFT, Sarnoff Imaging) captured aerial images of the retina whose acquisition was triggered with a mechanical shutter. This CCD is a frame transfer camera with a light sensitive area of 1,024 512 pixels. During each 500 ms exposure, continuous images of the retina are collected  $\times$  at a frame rate of 167 fps with 6 ms exposure.

Because of non-uniformity in gain across the CCD array and circuitry artifacts with the Sarnoff camera, background correction is necessary. Figure 35.1a shows a raw retinal image containing cone structure (object) and the Gaussian beam profile, CCD circuit and dust (noise). A background correction procedure was developed to correct these artifacts. Figure 35.1b shows a 'defocused image', which includes only noise. Correction of the raw retinal image for noise, and subsequent registration of multiple frames, results in the image in Figure 35.1c.

The position of cone photoreceptors in the adaptive optics images were identified using previously described automated Matlab software (Li and Roorda 2007) and manual identification by two of the authors. Cone density was measured using previously described methods (Carroll et al. 2004).

### 35.2.3 Spectral Domain Optical Coherence Tomography

In addition to the patient with the *LIA VAM* opsin, SD-OCT imaging was performed in 60 normal subjects (30 male, 30 female), ranging in age from 20 to 49 years-old, with a mean of 34.5 years. A Zeiss IOL Master (Dublin, CA) was used to measure axial length of each eye, and SD-OCT scan lengths were corrected for inter-individual differences in axial length based on Leung et al. (2007). Axial length in our subjects ranged from 21.96 to 29.93 mm, as such actual macular scan lengths ranged from 3.68 to 5.01 mm. The SD-OCT imaging protocol included a fast volume scan (512 A scans/B scan; 50 B scans in a nominal 4 4 mm volume). Additional high-resolution line scans were obtained (1,000 A-scans/B  $\times$  scan; 100 repeated line scans) through the center of fixation, which was cross-referenced with the volumetric scan to ensure coincidence with the foveal pit. Scans from each eye were directly exported and read into ImageJ (<http://www.rsb.info.nih.gov/ij/>) for processing. Frames from scans that were distorted due to large saccades or eye blinks were removed. A rigid body registration using the ImageJ plugin 'StackReg' was applied to generate a stabilized frame sequence for subsequent averaging (Thévenaz et al. 1998). The internal limiting membrane (*ILM*), outer plexiform layer (*OPL*), external limiting membrane (*ELM*) and retinal pigmented epithelium (*RPE*) were manually segmented. The distance between the ILM and RPE provided total retinal thickness while the distance between the OPL and ELM provided the outer nuclear layer (ONL) thickness.

## 35.3 Results

### 35.3.1 Cone Photoreceptor Mosaic Topography

To determine whether there were any structural changes since the initial imaging, three patches of retina between 1 and 1.5° temporal eccentricity were subject to detailed analysis. In order to make a direct comparison of cone locations, we first precisely co-registered the image from the initial imaging session to that from the most recent session (as the images were acquired on different adaptive optics cameras, the retinal magnification was different). Shown in Fig. 35.2a is an image from 1.25° temporal retina taken in November 2008. Figure 35.2b shows an overlay of identified cone coordinates, the cone density at this location is

21,367 cones/mm<sup>2</sup>. Figure 35.2c shows a comparison of cone coordinates from this patch of retina from the initial and most recent imaging sessions. Over this period spanning nearly 6 years, there has been virtually no change in the microstructure of the mosaic, as indicated by the close agreement of cone positions. This analysis was repeated on two other retinal locations and the average discrepancy between images was only 832 cones/mm<sup>2</sup> (the equivalent of five cone misidentifications). Owing to the high contrast and low spatial frequency of the gaps in the cone mosaic, it was qualitatively determined that the same gaps present in the initial images still remain (*data not shown*).

To quantitatively evaluate the gross topography of the cone mosaic, we compared cone density between the two imaging sessions. Figure 35.2d shows cone density as a function of retinal eccentricity for patient NC compared to normals. Compared to imaging (Carroll et al. 2005) and histology (Curcio et al. 1990) data from normal retina, patient NC has dramatically reduced cone density. There is an approximate 35% reduction in cone numerosity across the central retina. However, the precipitous decline in density from the fovea remains, with the curve shifted vertically, suggesting that normal cone migration and foveal packing took place. Also shown in Fig. 35.2d is the density curve from the initial evaluation (January 2003). Compared to the most recent examination, cone density appears unchanged, suggesting that the morphological disruption we observed is static in nature over at least a 6-year period.

### 35.3.2 Outer Nuclear Layer Thickness

Previous work has shown significant variation in 'normal' ONL thickness (Jacobson et al. 2007; Jacobson et al. 2005). We also observed significant variability in ONL thickness among the 60 normal subjects (Fig. 35.3a). The ONL thickness is greatest under the foveal pit, and falls off by nearly half by 2 mm eccentricity, reflecting the significant non-uniformity in cone density across the macular region (Curcio et al. 1990). Interestingly in the patient with the *LIAVA M* opsin there was no abnormality observed on the SD-OCT (Fig. 35.3b), despite the reduction in cone numerosity observed with adaptive optics.

## 35.4 Discussion

Based on the packing density of the cone photoreceptors, one would predict that the ONL thickness should be dependent on the number of photoreceptors present. Therefore it is curious that despite an apparent reduction in cone number in the *en face* AO images, no disruption in the SD-OCT was observed. One possible explanation is that the ONL thickness is maintained by glial cells, much like how RNFL thickness remains normal in RP patients despite significant axonal loss (Hood et al. 2009). Alternatively, it is possible that affected cone cells have not completely degenerated and their cell bodies remain in the ONL layer. However, we do know that even if structurally present, these cones are not contributing to function as seen by both the dichromatic phenotype (Carroll et al. 2004) and AO microperimetric findings (Makous et al. 2006). More generally, the disconnect between the AO and SD-OCT results suggests that a 'normal' OCT image does not necessarily imply that there is normal function of the retina. As shown here, cellular damage of the photoreceptors can still exist, and this warrants further investigation for determining the absolute sensitivity of both imaging modalities. This study highlights the potential utility of using SD-OCT to aid in the interpretation of AO. There is also clinical value in using AO to decipher SD-OCT abnormalities, however the full diagnostic potential of this relationship has yet to be realized, though integration with functional measures will aid in this effort (Choi et al. 2006; Duncan et al. 2007).

## Acknowledgments

The authors thank Dr. Alf Dubra for technical assistance with the adaptive optics control software & Dr. Tom Connor for helpful discussion. This study was supported by NIH Grants EY017607, EY001931, & EY014537, Fight for Sight, The E. Matilda Ziegler Foundation for the Blind, The Karl Kirchgessner Foundation, the RD & Linda Peters Foundation, the Gene & Ruth Posner Foundation, and an unrestricted departmental grant from Research to Prevent Blindness. JC is the recipient of a Career Development Award from Research to Prevent Blindness.

## References

- Carroll J, Neitz M, Hofer H, et al. Functional photoreceptor loss revealed with adaptive optics: an alternate cause for color blindness. *Proc Natl Acad Sci USA*. 2004; 101(22):8461–8466. [PubMed: 15148406]
- Carroll J, Porter J, Neitz J, et al. Adaptive optics imaging reveals effects of human cone opsin gene disruption. *Invest Ophthalmol Vis Sci*. 2005; 46 ARVO E-Abstract:4564.
- Choi SS, Doble N, Hardy JL, et al. In vivo imaging of the photoreceptor mosaic in retinal dystrophies and correlations with visual function. *Invest Ophthalmol Vis Sci*. 2006; 47(5):2080–2092. [PubMed: 16639019]
- Curcio CA, Sloan KR, Kalina RE, et al. Human photoreceptor topography. *J Comp Neurol*. 1990; 292:497–523. [PubMed: 2324310]
- Deeb SS, Lindsey DT, Hibiya Y, et al. Genotype-phenotype relationships in human red/green color-vision defects: molecular and psychophysical studies. *Am J Hum Genet*. 1992; 51:687–700. [PubMed: 1415215]
- Duncan JL, Zhang Y, Gandhi J, et al. High-resolution imaging with adaptive optics in patients with inherited retinal degeneration. *Invest Ophthalmol Vis Sci*. 2007; 48:3283–3291. [PubMed: 17591900]
- Fernández EJ, Vabre L, Hermann B, et al. Adaptive optics with a magnetic deformable mirror: Applications in the human eye. *Opt Express*. 2006; 14(20):8900–8917. [PubMed: 19529270]
- Hayashi T, Motulsky AG, Deeb SS. Position of a ‘green-red’ hybrid gene in the visual pigment array determines colour-vision phenotype. *Nat Genet*. 1999; 22:90–93. [PubMed: 10319869]
- Hood DC, Lin CE, Lazow MA, et al. Thickness of receptor and post-receptor retinal layers in patients with retinitis pigmentosa measured with frequency-domain optical coherence tomography (fdOCT). *Invest Ophthalmol Vis Sci*. 2009; 50(5):2328–2336. [PubMed: 19011017]
- Jacobson SG, Aleman TS, Cideciyan AV, et al. Human cone photoreceptor dependence on RPE65 isomerase. *Proc Natl Acad Sci USA*. 2007; 104(38):15123–15128. [PubMed: 17848510]
- Jacobson SG, Aleman TS, Cideciyan AV, et al. Identifying photoreceptors in blind eyes caused by RPE65 mutations: Prerequisite for human gene therapy success. *Proc Natl Acad Sci USA*. 2005; 102(17):6177–6182. [PubMed: 15837919]
- Jagla WM, Jägle H, Hayashi T, et al. The molecular basis of dichromatic color vision in males with multiple red and green visual pigment genes. *Hum Mol Genet*. 2002; 11:23–32. [PubMed: 11772996]
- Leung CK, Cheng ACK, Chong KKL, et al. Optic disc measurements in myopia with optical coherence tomography and confocal scanning laser ophthalmoscopy. *Invest Ophthalmol Vis Sci*. 2007; 48(7):3178–3183. [PubMed: 17591887]
- Li KY, Roorda A. Automated identification of cone photoreceptors in adaptive optics retinal images. *J Opt Soc Am A Opt Image Sci Vis*. 2007; 24(5):1358–1363. [PubMed: 17429481]
- Makous W, Carroll J, Wolfing JI, et al. Retinal microscotomas revealed with adaptive-optics microflashes. *Invest Ophthalmol Vis Sci*. 2006; 47(9):4160–4167. [PubMed: 16936137]
- Nathans J, Piantanida TP, Eddy RL, et al. Molecular genetics of inherited variation in human color vision. *Science*. 1986; 232:203–210. [PubMed: 3485310]
- Neitz M, Carroll J, Renner A, et al. Variety of genotypes in males diagnosed as dichromatic on a conventional clinical anomaloscope. *Vis Neurosci*. 2004; 21:205–216. [PubMed: 15518190]
- Rha J, Jonnal RS, Thorn KE, et al. Adaptive optics flood-illumination camera for high speed retinal imaging. *Opt Express*. 2006; 14(10):4552–4569. [PubMed: 19516608]

- Thévenaz P, Ruttimann UE, Unser M. A pyramid approach to subpixel registration based on intensity. *IEEE Trans Image Process.* 1998; 7(1):27–41. [PubMed: 18267377]
- Ueyama H, Li Y-H, Fu G-L, et al. An A-71C substitution in a green gene at the second position in the red/green visual-pigment gene array is associated with deutan color-vision deficiency. *Proc Natl Acad Sci USA.* 2003; 100(6):3357–3362. [PubMed: 12626747]
- Z136 ASC. American national standard for safe use of lasers. Orlando: 2007.

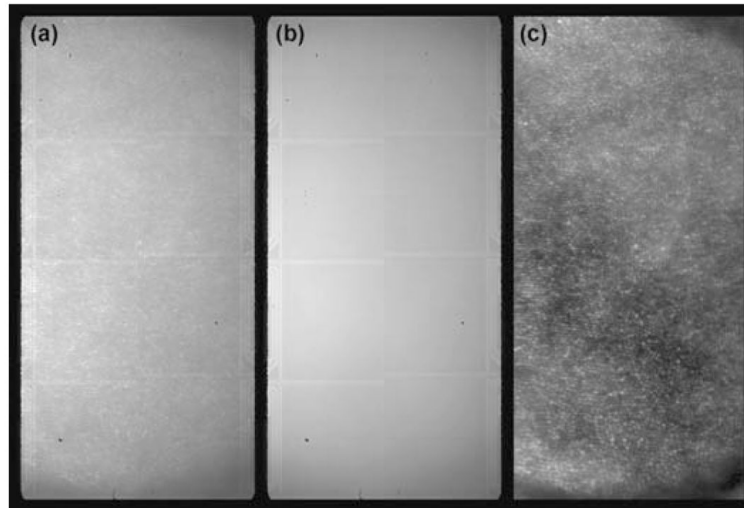


**Fig. 35.1.** Processing retinal images from the Medical College of Wisconsin Adaptive Optics Ophthalmoscope. **(a)** Raw image from the CCD camera ( $\sim 1.8^\circ \times \sim 0.9^\circ$ ). **(b)** Noise image comprised of dust, beam profile, and CCD circuit. **(c)** Processed retinal image (noise removed, registered average of 20 individual frames)

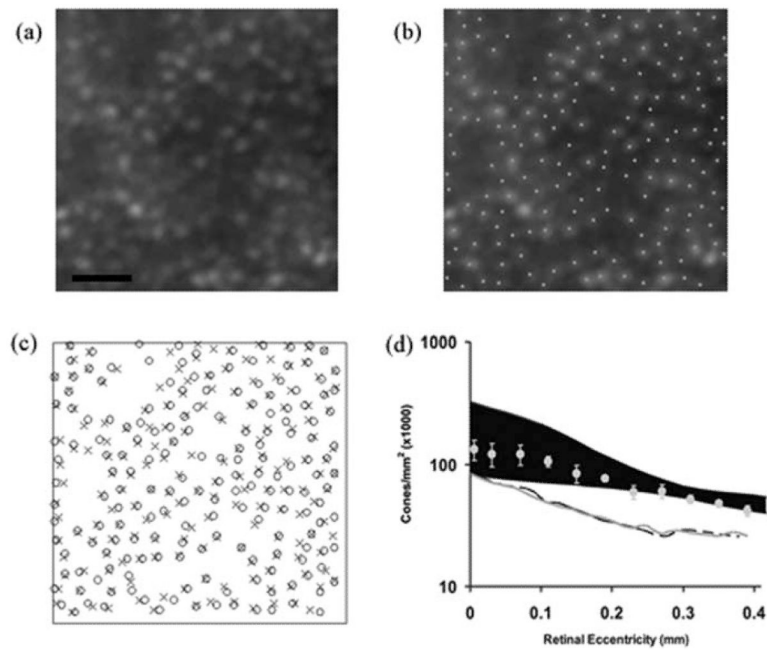


**Fig. 35.2.**

Longitudinal imaging of the cone mosaic in the LIAVA retina. **(a)** Cone mosaic image from 1.25° temporal retina, taken November 2008 on the Medical College of Wisconsin Adaptive Optics Ophthalmoscope. Scale bar = 20 microns **(b)** Same image as in **(a)**, with cone locations identified as *dots*. **(c)** Comparison of cone locations in **(b)** (*crosses*) to that from the exact same retinal location taken about 6 years prior (*open circles*). **(d)** Plot of cone density as a function of eccentricity. *Shaded region* represents normal bounds from histology data (Curcio et al. 1990) and *filled circles* represent average  $\pm 1$  SD values from adaptive optics data (Carroll et al. 2005). Density data for patient NC is plotted as a *black dashed line* (November 2008) and a *gray line* (January 2003)

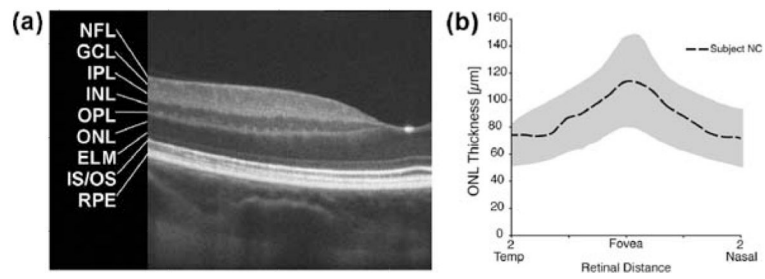


**Fig. 35.3.**

SD-OCT imaging in the *LIA VA* retina. **(a)** Line scan through the central fovea of patient NC, main retinal layers are labeled: NFL nerve fiber layer, GCL layer, = ganglion cell IPL = inner plexiform INL = inner nuclear = layer, OPL outer plexiform layer, ONL outer nuclear layer, ELM = external limiting membrane, IS/OS = = junction, = inner/outer segment RPE = retinal pigment epithelium. **(b)** ONL thickness across horizontal meridian in normal subjects (*shaded gray*,  $\pm 2$  SD) and patient NC with *LIA VA* M-opsin (*dashed black line*). Thickness data is presented as right eye equivalents